Reviewer 2

We would like to thank Reviewer #2 for his/her review of our paper and the important comments and suggestions provided. Please, find below our responses to the Reviewer's comments and the details on how we address them in the new version of the manuscript

General comments.

The text is a bit hard to follow. It is highly recommended that the authors make an effort to shorten it and make the language and the message more succinct. The quality of the figures can be significantly improved as well. There are a few important points that need to be cleared in the next revision.

Thanks to the reviewer for the suggestion. We have shortened the manuscript and tried to make the message more succinct. We have also improved figures 2, 6, 7, 8, 11, and 14 (now Figures 13 and 16 because new Figures 9 and 11 have been added to address some comments by Reviewer 1) and the captions have been modified accordingly.

Figure 2:

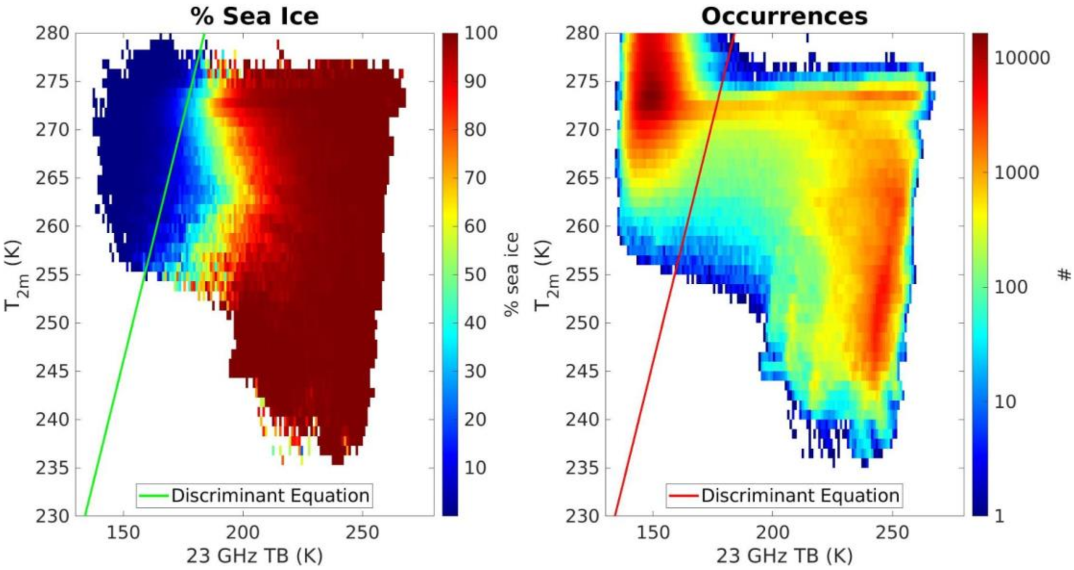

The caption has been changed

from:

Figure 2: Sea Ice Detection: 23 TB-T_{2m} Plan. The color represents the mean AutoSnow sea ice percentage within each bin (left) and the observation occurrence (right).

to

Figure 2: Sea Ice Detection: 23 TB-T_{2m} Plan. The color represents the mean AutoSnow sea ice percentage within each bin (left) and the observation occurrence (right). The green (left) and red (right) lines represent the discriminant Equation between sea ice and ocean.

For Figure 6, see answer to Comment 2.20.

Figure 7:

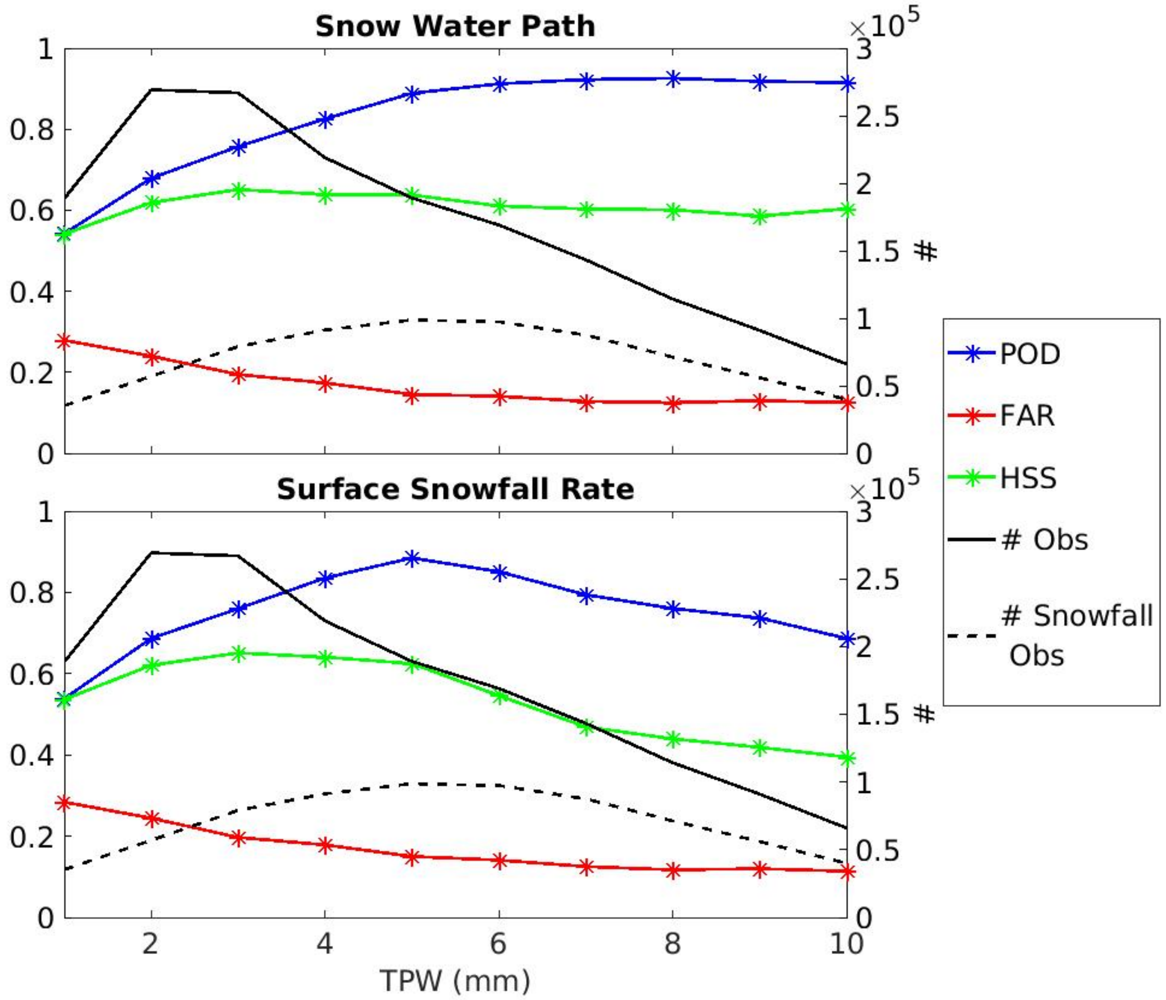

The caption has been changed

from:

Figure 7 HANDEL-ATMS SWP and SSR Detection Performances for different bins of TPW. The left y-axis reports POD, FAR and HSS vales, while the right y-axis reports the total number and snowfall observations in the dataset. POD-tot, FAR-tot and HSS-tot (dotted lines) represent the statistical scores estimated on the total dataset (values reported in Table 2).

to

Figure 7: HANDEL-ATMS SWP and SSR Detection Performances for different bins of TPW. The left y-axis reports POD, FAR and HSS vales, while the right y-axis reports the total number and snowfall observations in the dataset.

Figure 8:

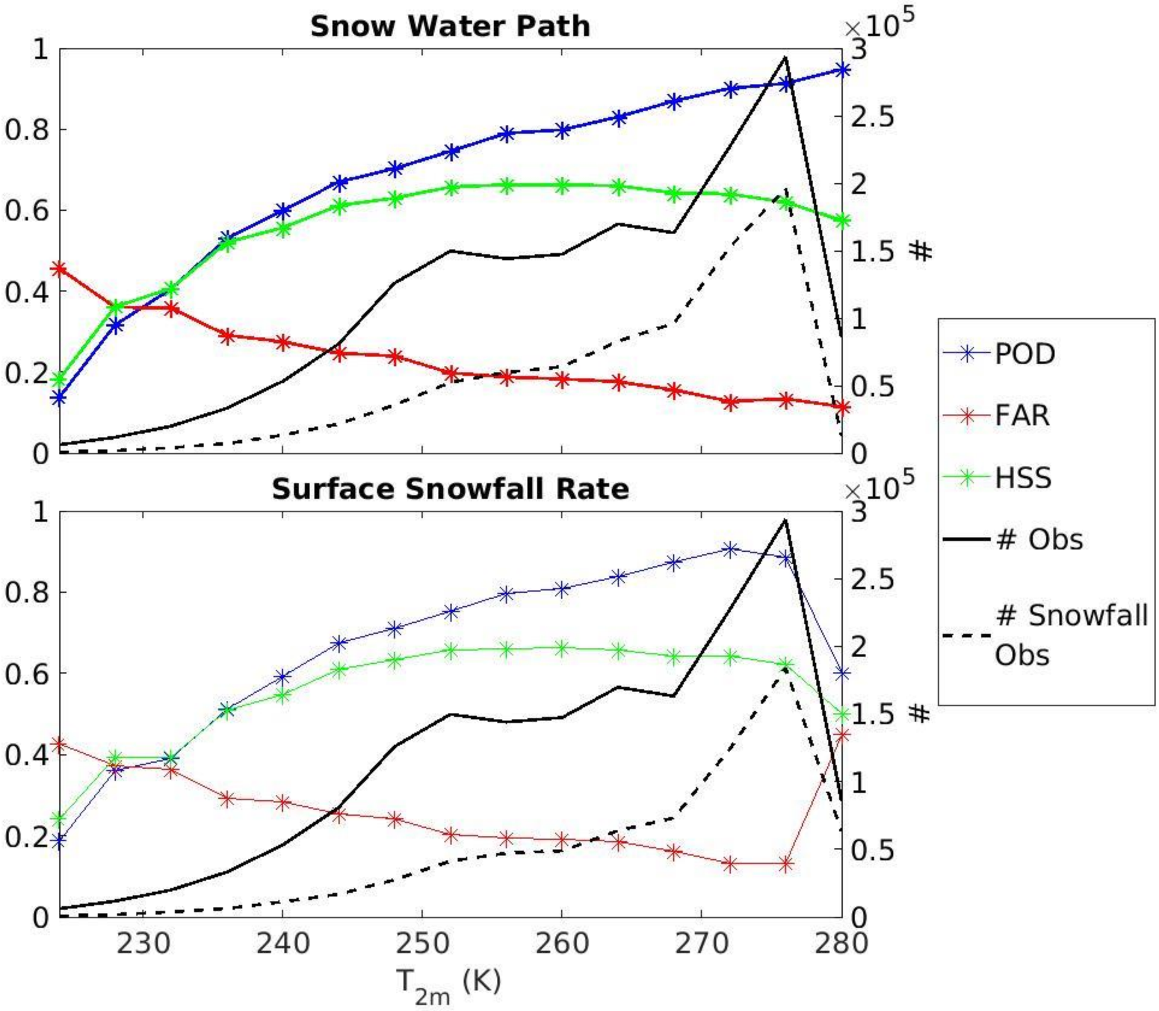

The caption has not been changed

Figure 11/13:

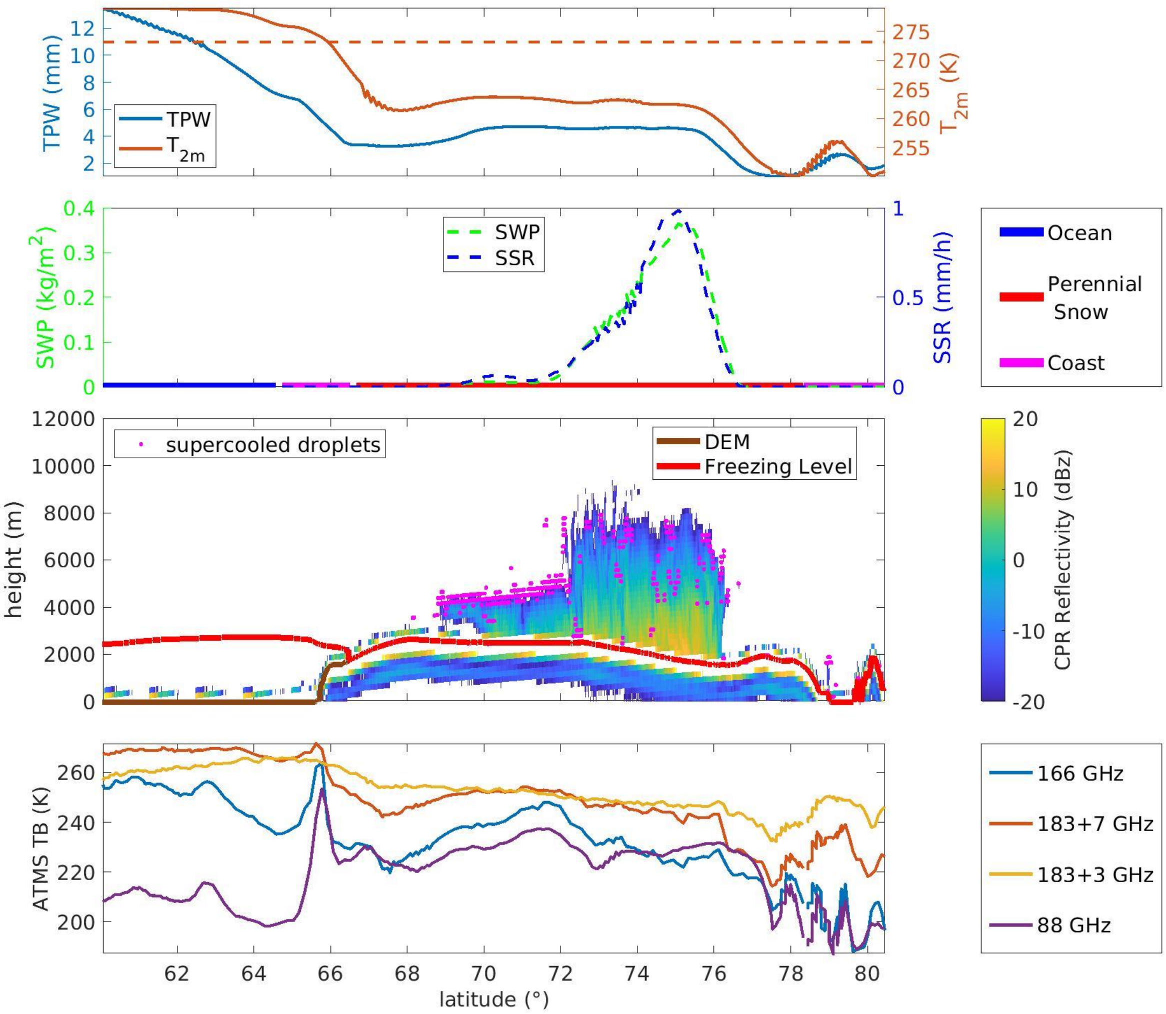

The caption has been changed

from:

Figure 11: Greenland - 2016/04/24 - Synopsis along CloudSat Track. The first panel shows the ECMWF TPW and T_{2m} values along the CloudSat track. In the second panel, the 2CSP SWP (left) and the SSR (right) values are reported, besides the PESCA classification along CloudSat track. In the third panel, the CPR reflectivity (values are reported in the colorbar below), the supercooled water droplets detected by DARDAR (magenta points) are shown. Also the Digital Elevation Model (brown line) and the ECMWF Freezing Level (red line) along CloudSat track are reported. In the bottom panel the observed TBs of the main high-frequency channels (88 GHz, 166 GHz, 183+3 GHz, 183+7 GHz) along CloudSat track are shown.

to

Figure 13: Greenland - 2016/04/24 - Synopsis along CloudSat Track. The first panel shows the ECMWF TPW and T_{2m} values along the CloudSat track. In the second panel, the 2CSP SWP (left) and the SSR (right) values are reported, besides the PESCA classification along CloudSat track. In the third panel, the CPR reflectivity (values are reported in the colorbar on the right), the supercooled water droplets detected by DARDAR (magenta points) are shown. Also the Digital Elevation Model (brown line) and the ECMWF Freezing Level (red line) along CloudSat track are reported. In the bottom panel the observed TBs of the main high-frequency channels (88 GHz, 166 GHz, 183+3 GHz, 183+7 GHz) along CloudSat track are shown.

Figure 14/16:

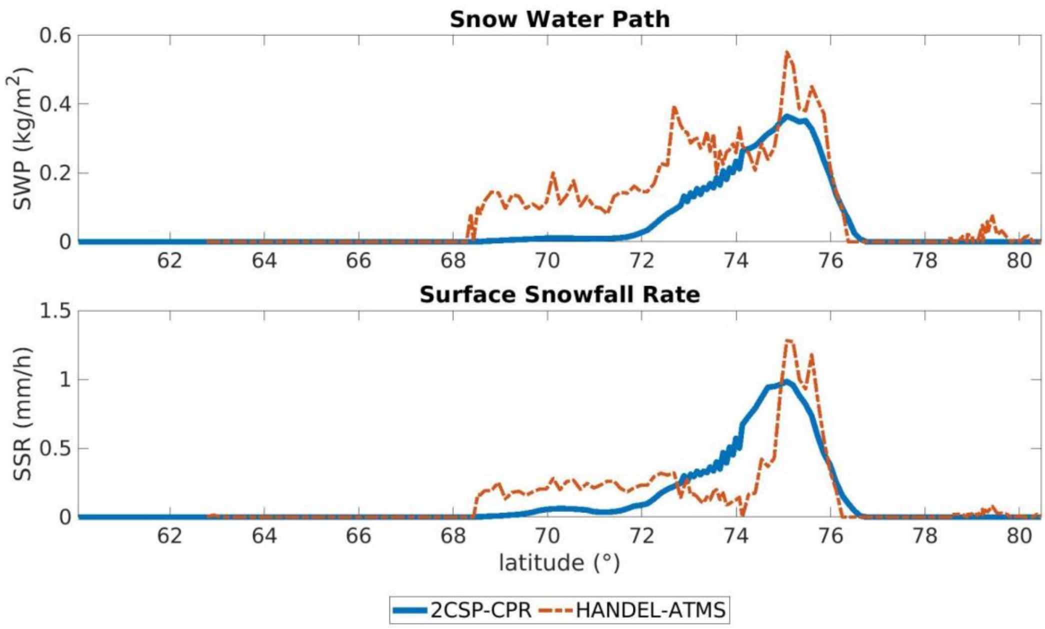

The caption has not been changed

For the new Figures 9 and 11, see answers to Comments 2.5 and 2.18.

2.1) The explanation of the inverse radiative transfer modeling is missing. Such an inversion can be significantly underconstrained and add additional uncertainty to the results.

Thanks to the reviewer for the comment. The model used is a plane-parallel approximation (see *Ulaby&Long, 2014*); the gas absorption model is that described by *Rosenkranz, 1998*. In particular, the emissivity has been calculated by inverting the radiative transfer equation

$$TB = T_{up} + (1 - \varepsilon) * T_{down} * e^{-\tau} + \varepsilon * T_{skin} * e^{-\tau}$$

to

$$\varepsilon = \frac{TB - T_{up} - T_{down} * e^{-\tau}}{e^{-\tau} * (T_{skin} - T_{down})}$$

where T_{up} represents atmospheric upward emission, T_{down} represents the atmospheric downward emission, τ represents the atmospheric optical thickness, ε represents the emissivity, T_{skin} represents the skin temperature and TB the ATMS observed TB. T_{up}, T_{down}, and τ are obtained by applying the Rosenkranz model using ECMWF-AUX temperature and water vapour profiles, T_{skin} is obtained from ECMWF-AUX product.

References:

Rosenkranz, P. W., Water vapor microwave continuum absorption: A comparison of measurements and models. *Radio Science*, *33*(4), 919-928. https://doi.org/10.1029/98RS01182, 1998.

Ulaby, F., & Long, D., Microwave radar and radiometric remote sensing, 1st Edition, the Univ. of Michigan Press, ISBN: 978-0-472-11935-6, 2014.

2.2) Please clarify upfront whether the estimated values of surface emissivities are used dynamically or statistically in the algorithm. Do they change in time or not?

Thanks to the reviewer for the comment. The emissivity values are retrieved for each pixel using the low-frequency TBs and environmental parameters at the time of the overpass; therefore, the emissivities are used dynamically. So the text has been changed:

Line 27:

from:

Moreover, their wide range of channel frequencies (from 23 GHz to 190 GHz), allows for the radiometric characterization of the surface at the time of the overpass along with the exploitation of the high-frequency channels for snowfall retrieval.

to:

Moreover, their wide range of channel frequencies (from 23 GHz to 190 GHz), allows for the dynamic radiometric characterization of the surface at the time of the overpass along with the exploitation of the high-frequency channels for snowfall retrieval.

Line 136:

from:

The present work has the aim to develop an algorithm for snowfall detection and estimation by exploiting the large frequency range typical of the last generation radiometers and to obtain a radiometric characterization of the background surface at the time of the satellite overpass in order to highlight the complex relationship between upwelling radiation and snowfall signature, which makes the detection very difficult in the typical conditions of the high latitudes.

to:

The present work has the aim to develop an algorithm for snowfall detection and estimation by exploiting the large frequency range typical of the last generation radiometers and to obtain a dynamic radiometric characterization of the background surface at the time of the satellite overpass in order to highlight the complex relationship between upwelling radiation and snowfall signature, which makes the detection very difficult in the typical conditions of the high latitudes.

2.3) It will be helpful if the authors clarify why we need land surface classification for the algorithm. For example, there are multiple products for the detection of the presence of snow and sea ice dynamics using optical bands (every 30 minutes). These optical products can be more accurate than microwave classification schemes, in terms of the presence or absence of frozen surfaces. Why we should not use them?

Thanks to the reviewer for the question. There are indeed multiple products for snow-cover and sea ice detection. However, PESCA aim is to obtain information ancillary to the snowfall retrieval at the time of the overpass, by exploiting the same instruments and the same type of data which will be used downstream for snowfall retrieval (see *Camplani et al, 2021*). We are more interested in the emissivity spectrum in the microwave than in very accurate and high-resolution snow and sea ice detection. Moreover, products based on optical observations are unreliable in presence of clouds, while our goal is to use them to retrieve cloud properties. To our knowledge, the only product available every 30 min comes from geostationary satellites that show several limitations in observing high latitudes.

References:

Camplani, A., Casella, D., Sanò, P., & Panegrossi, G.: The Passive microwave Empirical cold Surface Classification Algorithm (PESCA): Application to GMI and ATMS. *Journal of Hydrometeorology*, *22*(7), 1727-1744,https://doi.org/10.1175/JHM-D-20-0260.1, 2021.

2.4) From a methodological standpoint, the explanations of neural networks need to be improved. A the same time, the use of linear discriminant analysis seems outdated in light of the new deep-learning classification models.

Thanks to the reviewer for the comment. We know that deep-learning classification models are more effective than models based on other machine learning approaches, such as linear discriminant analysis. However, our goal was to obtain a classification scheme preliminary to the snowfall retrieval modules, and so we have chosen to use methods which are simple and not too computationally and time consuming.

2.5) While the paper focuses on different land surface types and sea ice ages, it is unclear how statistically significant the presented results are in Table 7. The number of training and testing samples needs to be clarified.

Thanks to the reviewer for the suggestion. We believe that the reviewer is referring to Table 6. We have replaced it with Figure 9. In the two plots the statistical scores for each class, the total observation number and the snowfall observation number for the test phase are reported. For what concerns the number of training and testing samples, see answer to Comment 2.6.

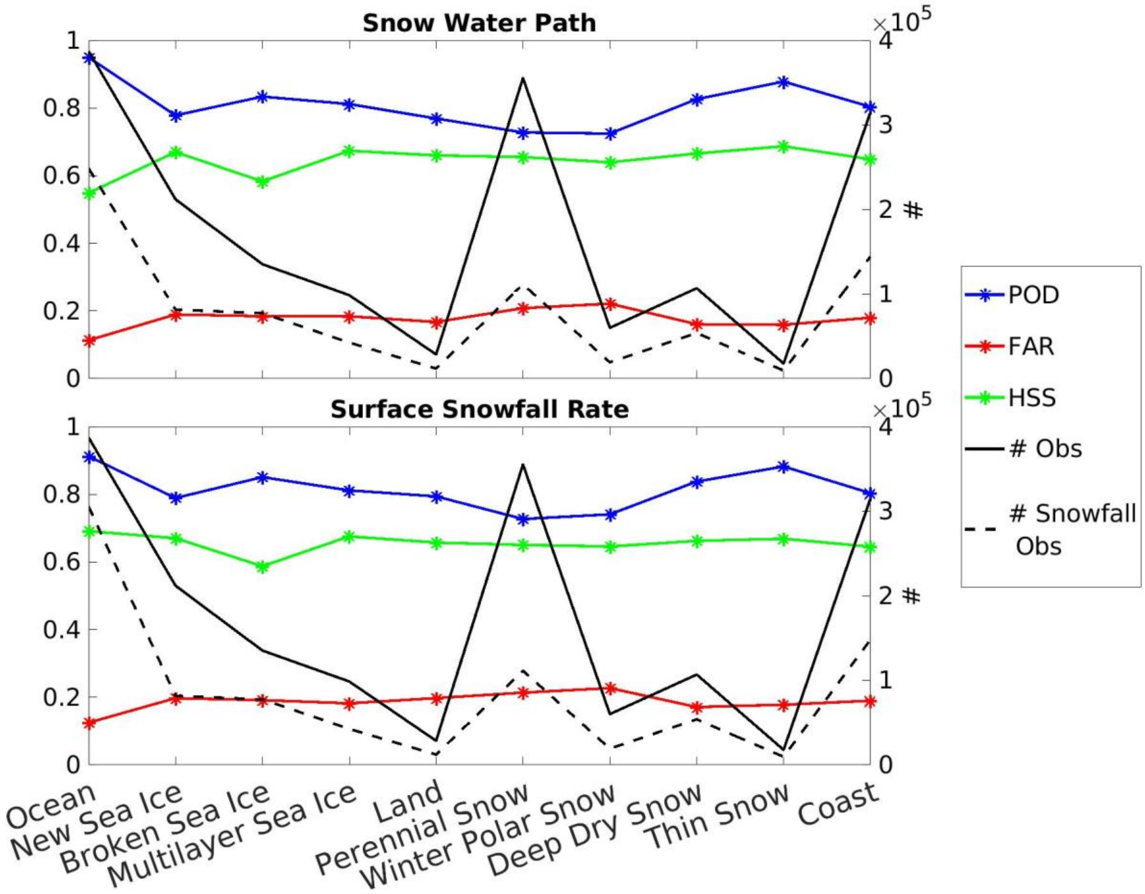

Figure 9: Same as Figure 7 but for PESCA surface classes.

The violet continuous and dashed line represents the total class occurrence and the snowfall occurrence for each class respectively. So, it is possible to observe that also the less populated classes, such as Thin Snow, are characterized by about $3*10^4$ total observations and $1*10^4$ snowfall observations. So the statistics can be considered statistically significant. This Figure has been added to the manuscript.

2.6) It would benefit the paper if the authors provide the entire confusion matrix of the detection of snowfall, including, recall, precision, and accuracy.

Thanks to the reviewer for the suggestion. Here the confusion matrices and the precision, recall and accuracy values are reported.

SWP detection - Confusion Matrix		
HANDEL/2CSP	**YES**	**NO**
YES	**606711**	**106407**
NO	**106541**	**581671**

precision=0.85

recall=0.85

accuracy=0,84

SSR detection - Confusion Matrix		
HANDEL/2CSP	**YES**	**NO**
YES	**541688**	**102542**
NO	**113615**	**643485**

precision=0.82

recall=0.84

accuracy=0,84

The total number of observations is $1,40*10^{6}$, which corresponds to about ⅔ of the total observations number. A similar proportion can be observed for the SWP and SSR observations. The following statement has been added to the text (line 223):

In this work, the dataset has been filtered based on humidity (TPW < 10 mm) and temperature (T_{2m} <280 K) conditions (the working limits of the PESCA algorithm, see Camplani et al, 2021) leading to a good representation of the higher latitudes with 80 % of the dataset elements located above 60°N/S. are . The dataset is made of $2,14*10^{6}$ elements, including $1,07*10^{6}$ elements with falling snow (2CSP SWP > kg/m2) and $9,99*10^{5}$ with snowfall at the surface (2CSP SSR > 0 mm/h) . The training and test phases have been conducted by splitting randomly the dataset, with ⅓ of the elements in the training and ⅔ of the elements in the test dataset.

Therefore, data about the dataset dimension, the training and test phase and the snowfall have been added to the text. We would prefer not to add the confusion matrices to the text in order to avoid further lengthening the manuscript. We think that the information about the dataset, joined with the statistical scores, shows a comprehensive picture of the study. At the same time, the recall gives the same information of POD, and precision can be considered the complementary value to 1 of the FAR. The information linked to the accuracy can be misleading: so we would prefer to keep in the text only the information about POD, FAR and HSS.

Detail comments:

2.7) Section 2.4 is long and has some generic explanations about for example neutral networks, which is not necessary at this time. It is recommended to shorten the text.

Agreed. The text has been shortened (see answer to Comment 2.8).

2.8) The explanation of the architecture of the neural network is weak. First of all the networks use the Levenberg-Marquardt algorithm which is extremely old and is not being used in modern training of deep neural networks. Unlike algorithms like Adam, it is prone to get stuck in local minima and suffer from the vanishing gradient problem.

We agree with the reviewer that the LM algorithm is outdated and it is not being used in deep neural network training. Our point here is that our networks are shallow, as written in section 3.2 of the manuscript:

The snowfall detection and estimation modules have been based on ANNs. Four ANNs have been developed: two for the detection of SWP and SSR and two for the SWP and SSR estimate. The performance of more than 50 architectures have been tested, by varying the number of layers, the number of neurons for each layer, and the activation functions. The final architecture, for all modules, is composed of four layers: an input layer with a neurons number equal to the predictor number, and a hyperbolic tangent function as the activation function, a first hidden layer (60 neurons), and hyperbolic tangent function, a second hidden layer (30 neurons), with a logarithmic tangent function.

Therefore, the neural networks described in this paper are composed of less than 150 weights. These networks fall into the category of feed forward, or multilayer perceptron networks, or shallow neural networks. The LM optimizer is prone to several issues when the depth of the network grows (i.e. if the number of weights to be trained is higher than about 500, see *Yu & Wilamowski, 2018*), such as gradient vanishing, however it has been proven to be a very accurate optimizer for shallow neural networks. The use of the LM optimizer forces the choice of the error function, that needs to be the mean squared error, in regression problems, and may result slower than other optimizers, however it has proven to reach higher accuracy in many problems, even in very recent papers, in particular we followed the *Hagan&Menhaj, 1994* implementation of the LM algorithm that has been cited in about 700 papers after 2022 (see the google scholar link to recent citation of this paper). Moreover, we did test the impact of the choice of the optimizer for one of the neural networks module of the HANDEL-ATMS algorithm, and the results confirmed the use of the LM optimizer as an optimal choice for the complexity of the networks that we are training and for the size of the dataset that we are using. In particular the LM optimizer resulted to be more accurate but slower than other optimizers (including the Conjugate-gradient, gradient descend with momentum and Adam optimizers).

About the first point raised by the reviewer “The explanation of the architecture of the neural network is weak”, we believe that He/She is referring to section 2.4.1, that was intended as a brief introduction, and that has been modified

from:

2.4.1 Artificial Neural Networks

An Artificial Neural Network (ANN) is an information-processing system inspired by the functioning of biological neural networks. It is composed of neurons, i. e., elements where the information is processed using an activation function, and the connecting links between the neurons, where a weight multiplies the deriving from the upstream signal. In particular, the HANDEL-ATMS snowfall detection and estimation modules have been developed using feedforward multilayer neural network architectures, i. e., a neural network architecture where the neurons are arranged in layers; each neuron belonging to a layer receives, as input to its transfer function, a weighted sum of the outputs of the previous layer. This architecture, which is defined by the number of layers, the number of neurons for each layer, and the transfer function of each neuron, has to be designed beforehand. The weights of connection links and the bias values for each layer are estimated with a training process, based on the Levenberg–Marquardt algorithm (see Sanò et al, 2015)

to:

2.4.1 Artificial Neural Networks

The HANDEL-ATMS snowfall detection and estimation modules have been developed using feedforward multilayer neural network architectures, i. e., a neural network architecture where the neurons are arranged in layers. This architecture, which is defined by the number of layers, the number of neurons for each layer, and the transfer function of each neuron, has to be designed beforehand. The weights of connection links and the bias values for each layer are estimated with a training process, based on the Levenberg–Marquardt algorithm (see Sanò et al, 2015). The specific networks architecture, and the training and optimization procedure of the HANDEL-ATMS algorithm are described in detail in section 3.2.

References:

Yu, H., & Wilamowski, B. M.: Levenberg–marquardt training. In *Intelligent systems* (pp. 12-1), CRC Press, ISBN 9781315218427, 2018.

Hagan, M. T., & Menhaj, M. B.: Training feedforward networks with the Marquardt algorithm, *IEEE transactions on Neural Networks*, *5*(6), 989-993, DOI: 10.1109/72.329697, 1994.

2.9) Line 424–445 It is unclear how the detection and estimation networks are implemented. What are the cost functions? This must be clarified.

Thanks to the reviewer for the suggestion. The cost function is a sum of squares error (SSE) given by the following equation:

$$E = \frac{1}{n}\sum_{i=1}^{n} (y_i - t_i)^2$$

where y represents the output of the neural networks, and t represents the reference truth value. The characteristics of this Neural network approach have been largely described by *Sanò et al, 2015*, doi:10.5194/amt-8-837-2015). So, a reference to this paper has been added (line 431):

(for more information about the Neural Network characteristics, see Sanò et al, 2015)

References:

Sanò, P., Panegrossi, G., Casella, D., Di Paola, F., Milani, L., Mugnai, A., Petracca, M., & Dietrich, S.: The Passive microwave Neural network Precipitation Retrieval (PNPR) algorithm for AMSU/MHS observations: description and application to European case studies. *Atmospheric Measurement Techniques*, *8*(2), 837-857, https://doi.org/10.5194/amt-8-837-2015, 2015.

2.10) Line 345-346: It is not well-described how the inverse radiative transfer model is used. What is the forward RT model?

Thanks to the reviewer for the question. The simulations are based on a plane-parallel approximation (see *Ulaby, 2014)* and the gas absorption model is described by *Rosenkranz, 1998*. The text has been modified (see answer to Comment 1.15).

The text has been modified

from:
The RMSE between simulated clear-sky TBs - based on the mean emissivity values estimated for each class - and the coincident observed clear-sky TBs appears to be too high to implement a robust signal analysis (>10 K).
to:
The clear-sky radiative transfer model simulations are based on the mean emissivity values estimated for each class, and simulated by using the plane-parallel approximation (Ulaby & Long, 2014) and the Rosenkrantz gas absorption model (Rosenkrantz, 1998) - The RMSE between simulated clear-sky TBs and the coincident observed clear-sky TBs appears to be too high to implement a robust signal analysis (>10 K).

The following reference has been added to the text (Line 756):

Rosenkranz, P. W., Water vapor microwave continuum absorption: A comparison of measurements and models. Radio Science, 33(4), 919-928. https://doi.org/10.1029/98RS01182, 1998.

References:

Rosenkranz, P. W., Water vapor microwave continuum absorption: A comparison of measurements and models. *Radio Science*, *33*(4), 919-928. https://doi.org/10.1029/98RS01182, 1998.

Ulaby, F., & Long, D., Microwave radar and radiometric remote sensing, 1st Edition, the Univ. of Michigan Press, ISBN: 978-0-472-11935-6, 2014.

2.11) Lines 362-365: How emissivity is used for calculating the simulated TBs? It seems recursive to use the observations to estimate the emissivity and then use it for retrievals. Please clarify whether the used emissivities are dynamic or static.

Thanks to the reviewer for the comment. The emissivity values are retrieved for each pixel and are used to estimate the simulated TBs. Only low-frequency channels are used to classify the observations (by using PESCA) and to retrieve an emissivity spectrum for the observations. Then, this spectrum has been used to estimate the TBs for all ATMS channels. So the process is not recursive. The emissivities are used dynamically because they have been calculated for each observation (see answer to Comment 2.2).

2.12) Table 3: The parameters mentioned in the table are different than the ones mentioned in the text in lines 435-437.

Thanks to the reviewer for the comment. The Table has been changed:

from:

Predictor Set	POD	FAR	HSS
$\Delta TB_{obs-sim}$	0.75	0.29	0.48
TB_{obs}	0.81	0.18	0.65
TB_{obs}+environmental var	0.82	0.17	0.68
$TB_{obs}+\Delta TB_{obs-sim}$	0.84	0.16	0.69

Table 3: HANDEL-ATMS SSR Detection Performance: Statistical scores for different Predictor Sets

to:

Predictor Set	POD	FAR	HSS
$\Delta TB_{obs-sim}$+ ancillary parameters	0.75	0.29	0.48
TB_{obs}+ ancillary parameters	0.81	0.18	0.65
TB_{obs}+environmental variables+ ancillary parameters	0.82	0.17	0.68
$TB_{obs}+\Delta TB_{obs-sim}$+ ancillary parameters	0.84	0.16	0.69

Table 3: HANDEL-ATMS SSR Detection Performance: Statistical scores for different Predictor Sets

Minor comments:

2.13) Line 273: It is better to mention all the variables that have been used for training the network here.

Thanks to the reviewer for the suggestion. The text has been changed
from:
Four ANNs are then applied to a predictor set consisting of ATMS TB_{obs}, $\Delta TB_{obs-sim}$, a surface classification flag, and other environmental and ancillary parameters.
to:
Four ANNs are then applied to a predictor set consisting of ATMS TB_{obs}, $\Delta TB_{obs-sim}$, a surface classification flag, and other ancillary parameters (elevation and ATMS viewing angle for the final version).

2.14) line 203-204: list of environmental and ancillary parameters is not presented in the dataset.

Thanks to the reviewer for the comment. The text has been changed
from:
Some model-derived variables have been added to the dataset to be used as ancillary variables.

to:
Some model-derived variables, specifically Total Precipitable Water (TPW), the 2-m Temperature (T_{2m}), the Skin Temperature, the freezing level height and the temperature and humidity profiles, have been added to the dataset to be used as ancillary parameters.

2.15) Line 356: "…for ocean and land respectively."

Thanks to the reviewer for the correction.

The text has been changed

from:

The estimated spectra are shown in Figure 4 and Figure 5 for the land and ocean classes, respectively.
to:
The estimated spectra are shown in Figure 4 and Figure 5 for ocean and land respectively.

2.16) Line 387: What is the used atmospheric radiative transfer model? Please spell out RTM.

Thanks to the reviewer for the comment. The model used is that described by *Rosenkranz, 1998*. The text has been modified

from:

An emissivity spectrum, (calculated as the mean of the emissivity values for each cluster), together with ECMWF temperature and water vapor profiles, is used as input in the RTM to simulate the clear-sky TBs.
to
*An emissivity spectrum, (calculated as the mean of the emissivity values for each cluster), together with ECMWF temperature and water vapor profiles, is used as input in the radiative transfer model (RTM) (*see*Ulaby & Long ,2014, Rosenkrantz, 1998) to simulate the clear-sky TBs.*

References:

Rosenkranz, P. W., Water vapor microwave continuum absorption: A comparison of measurements and models. *Radio Science*, *33*(4), 919-928. https://doi.org/10.1029/98RS01182, 1998.

Ulaby, F., & Long, D., Microwave radar and radiometric remote sensing, 1st Edition, the Univ. of Michigan Press, ISBN: 978-0-472-11935-6, 2014.

2.17) Table 2: What is the accuracy represented here? The accuracy of PESCA for surface classification?

Thanks to the reviewer for the comment. The accuracy represented here is the ratio between the number of observations where both SOM and LDA identify the same cluster and the total observations of the class.

2.18) Line 489: Remove the dot at the beginning of the sentence.

Thanks to the reviewer for the correction. The text has been largely modified to address some comments by Reviewer 1.

from:

. Generally, it can be observed that, although HANDEL-ATMS is able to detect extremely light snowfall events, it does not have the sensitivity to correctly estimate their intensity.

to:

Figure 11 shows the dependence of HANDEL-ATMS snowfall estimation error statistics, as well of SWP and SSR, on TPW . The curves represent the mean SWP or SSR computed for each 1-mm TPW bin, the RMSE and the relative bias (the ratio between the bias and the SWP/SSR mean value for each bin). TPW and snowfall intensity are strongly correlated. An increase of the absolute RMSE can be observed as TPW increases, and it is larger than the SWP/SSR mean value for TPW < 8 mm. A similar behavior can be observed by analyzing the dependence of HANDEL-ATMS snowfall estimation error statistics on T_{2m} *(not shown). A very moderate overestimation is observed for TPW < 8 mm and for lower SWP and SSR values (< 0.1 mm/h), with relative bias around 5%, (up to 8% only for extremely low TPW values and very low number of observations (see Figure 7)), while underestimation (relative bias up to -5%) is observed for higher TPW values and higher SWP and SSR values. So, it can be concluded that HANDEL-ATMS has good detection capabilities (also for extremely light snowfall) but it shows some limitations in correctly estimating its intensity, with slight overestimation of the very light snowfall typical of high latitudes.*

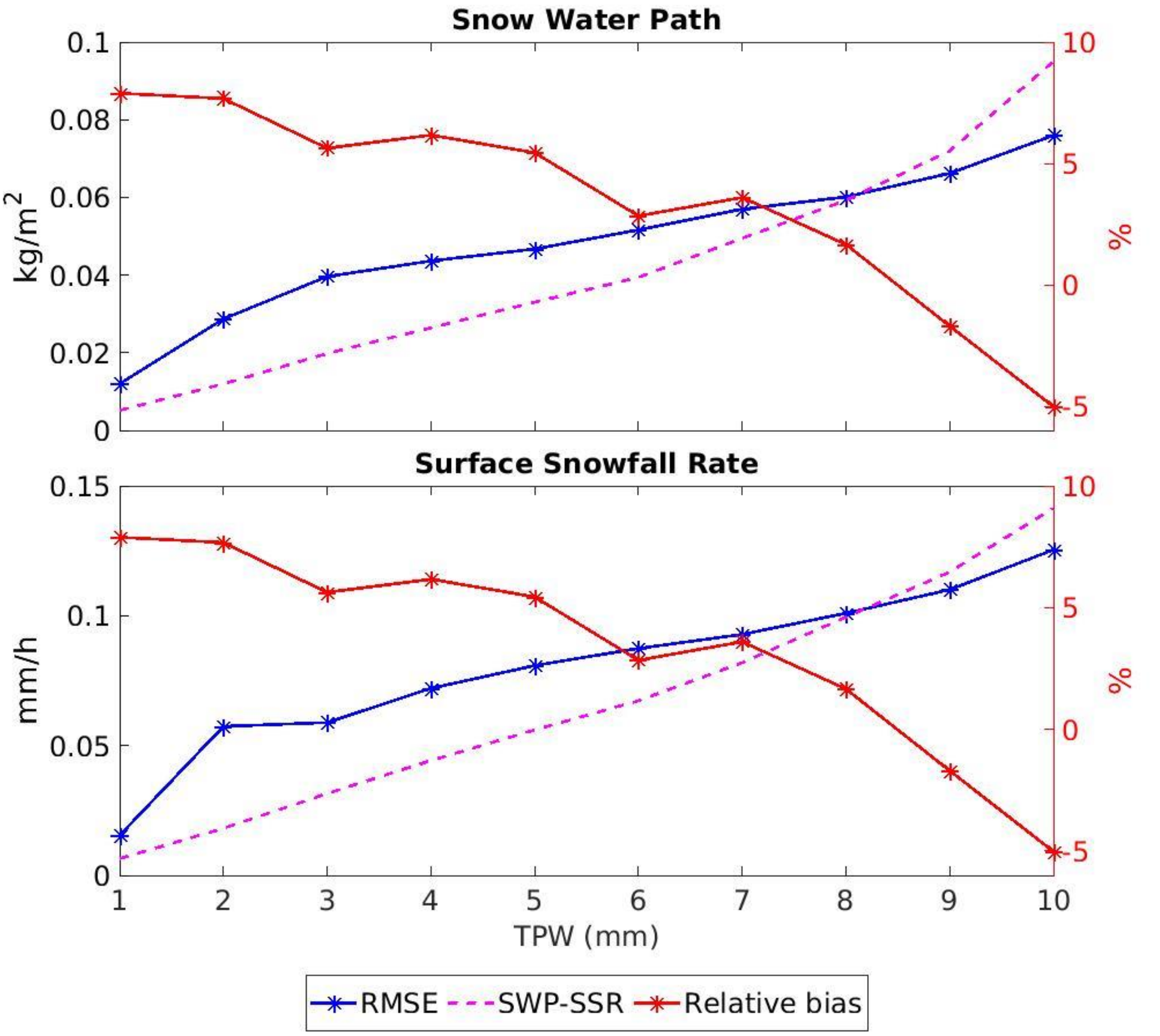

Figure 11: HANDEL-ATMS SWP and SSR Detection Performances for different bins of TPW. The left y-axis reports RMSE absolute values and the mean intensity value for each 1-mm TPW bin, while the relative bias, calculated as the ratio between the bias and the SWP/SSR mean value for each bin.

2.19) Figure 1: The inputs of PESCA mentioned in this figure are not aligned with the original paper. For example, there exists no explanation for the low-frequency ratio and scattering coefficients.

Thanks to the reviewer for the comment. Indeed, there is not a direct mention of the PESCA input parameters; however, these parameters are derived from the inputs cited in the box (low-frequency ratio is a ratio between two TB_{obs}, the scattering index is a difference between two TB_{obs}, pem_{LF} is a ratio between a TB_{obs} and T_{2m},see *Camplani et al, 2021*). We wanted to highlight that we use the same inputs in more than one module - e. g., TBs are used both for surface classification and snowfall detection and estimate. The same definition of the input variables of PESCA can be found in the paper in section 3.1.1.

References:

Camplani, A., Casella, D., Sanò, P., & Panegrossi, G.: The Passive microwave Empirical cold Surface Classification Algorithm (PESCA): Application to GMI and ATMS. *Journal of Hydrometeorology*, *22*(7), 1727-1744,https://doi.org/10.1175/JHM-D-20-0260.1, 2021.

2.20) Figure 6: No results are presented over sea ice.

Thanks to the reviewer for the comment.
Figure 6 has been modified, with two new subplots related to two PESCA classes (Ocean and New sea Ice).

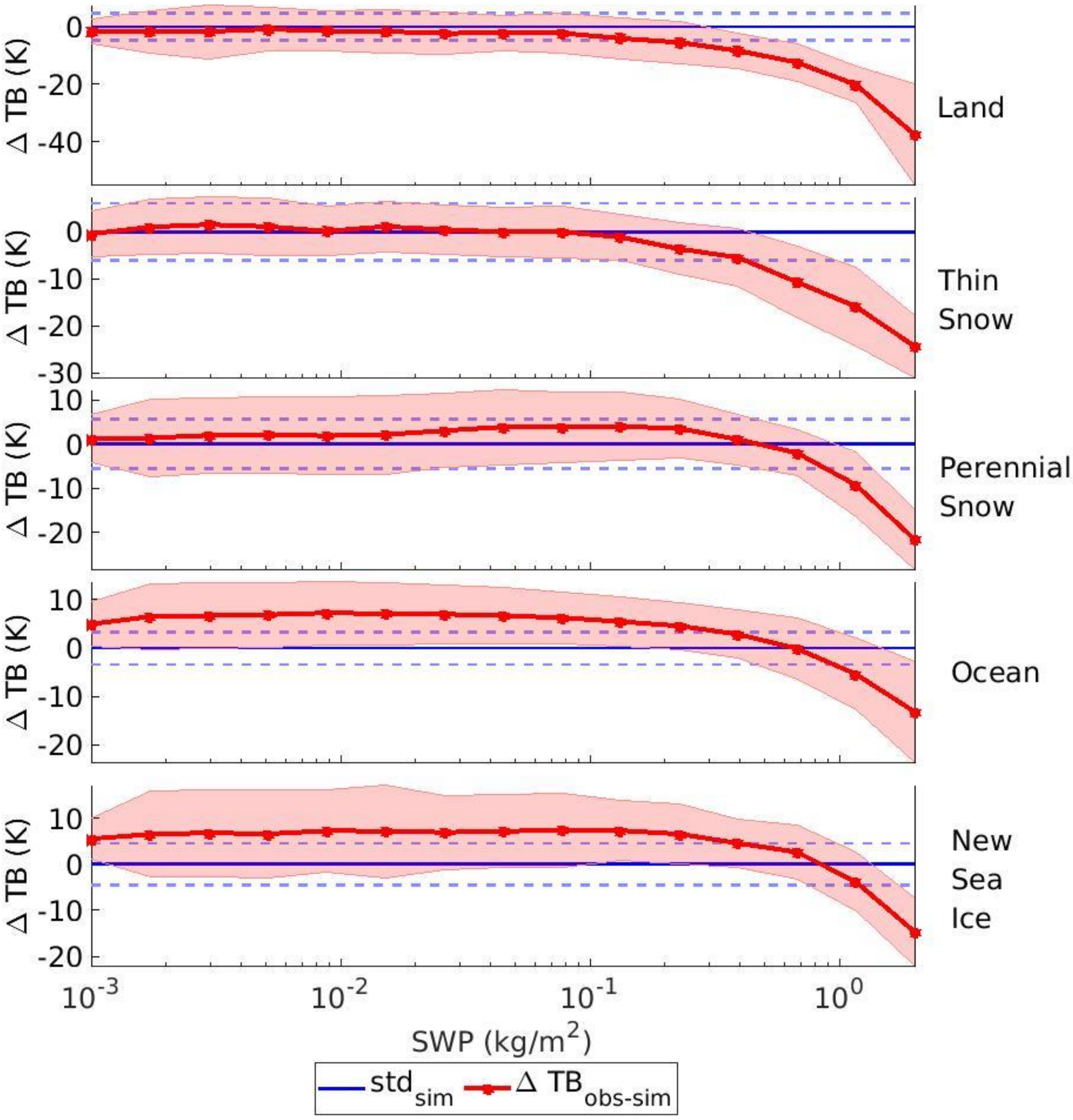

The following statement has been added to the text (line 423):

For what concerns ocean and new sea ice classes, a clear scattering signal is visible only for high SWP values (> 1 kg m^{-2}) while for low SWP values a significant emission signal is observed. The ubiquitous presence of supercooled water layers in snowing clouds (Wang et al, 2013, Battaglia & Panegrossi 2020), especially over oceans (Battaglia & Delanoe, 2013), generates an emission effect which is particularly significant over radiatively cold surfaces (such as Ocean and New Sea Ice at high frequency, see Figure 4), and can mask or overcome the weak scattering signal generated by falling snow especially in light snowfall events. It is also important to underline that the DARDAR product identifies only supercooled water layers at the cloud top (Panegrossi et al., 2017), while it has been shown that the impact of supercooled water layers embedded in the clouds can be very significant on the measured TBs at MW high frequency window channels (Battaglia & Panegrossi, 2020, Panegrossi et al., 2022) . It is very likely that the emission effect observed over ocean and sea ice is generated by supercooled liquid layers which are not identified by the DARDAR product.

Figure 6 caption has been modified accordingly

from:

> ***Figure 6: 165.5 GHz Snowfall Signature as a function of SWP for three Land surface Classes. The red line and shaded areas represent the mean values and standard deviations of $\Delta TB_{obs-sim}$ (i.e., the snowfall signature) while the blue lines are centered on the estimated bias and standard deviation of $\Delta TB_{obs-sim}$ in clear sky conditions for the corresponding PESCA surface class.***

to:

Figure 6: 165.5 GHz Snowfall Signature as a function of SWP for five PESCA surface classes. The red line and shaded areas represent the mean values and standard deviations of $\Delta TB_{obs-sim}$ (i.e., the snowfall signature) while the blue lines are centered on the estimated bias and standard deviation of $\Delta TB_{obs-sim}$ in clear sky conditions for the corresponding PESCA surface class.

The following reference has been added to the text (Line 798):

Wang, Y., Liu, G., Seo, E. K., & Fu, Y.: Liquid water in snowing clouds: Implications for satellite remote sensing of snowfall. Atmospheric research, 131, 60-72, https://doi.org/10.1016/j.atmosres.2012.06.008,2013.

References:

Battaglia, A., & Delanoë, J.: Synergies and complementarities of CloudSat-CALIPSO snow observations. *Journal of Geophysical Research: Atmospheres*, *118*(2), 721-731. https://doi.org/10.1029/2012JD018092, 2013.

Battaglia, A., & Panegrossi, G.: What can we learn from the CloudSat radiometric mode observations of snowfall over the ice-free ocean?. Remote Sensing, 12(20), 3285, https://doi.org/10.3390/rs12203285, 2020.

Panegrossi, G., Rysman, J. F., Casella, D., Marra, A. C., Sanò, P., & Kulie, M. S.: CloudSat-based assessment of GPM Microwave Imager snowfall observation capabilities. *Remote Sensing*, *9*(12), 1263, https://doi.org/10.3390/rs9121263, 2017.

Panegrossi, G., Casella, D., Sanò, P., Camplani, A., & Battaglia, A.: Recent advances and challenges in satellite-based snowfall detection and estimation. *Precipitation Science*, 333-376, https://doi.org/10.1016/B978-0-12-822973-6.00015-9, 2022.

Wang, Y., Liu, G., Seo, E. K., & Fu, Y.: Liquid water in snowing clouds: Implications for satellite remote sensing of snowfall. *Atmospheric research*, *131*, 60-72, https://doi.org/10.1016/j.atmosres.2012.06.008,2013.

2.21) Figure 10: Please mention that the shown green dots denote the CPR overpass.

Thanks to the reviewer for the suggestion. The caption of Figures 10 12, and 13 (now Figures 12, 14, and 15) has been changed

Figure 10/12:

from:

Figure 10: Greenland - 2016/04/24 - PESCA Background Surface Classification.

to:

Figure 12: Greenland - 2016/04/24 - PESCA Background Surface Classification. The green dotted line represents the CloudSat track.

Figure 12/14:

from:

Figure 12: Greenland - 2016/04/24 - 165 GHz Channel measured TB (TB_{obs}) (top panel) and the deviation of TB_{obs} from the simulated clear-sky TBs ($\Delta TB_{obs-sim}$) (bottom panel)

to:

Figure 14: Greenland - 2016/04/24 - 165 GHz Channel measured TB (TB_{obs}) (top panel) and the deviation of TB_{obs} from the simulated clear-sky TBs ($\Delta TB_{obs-sim}$) (bottom panel). The red dotted line (top panel) and the green dotted line (bottom panel) represent the CloudSat track.

Figure 13/15:

from:

Figure 13: Greenland - 2016/04/24 - Maps of the HANDEL-ATMS module's output: the SWP detection mask (top panel), the estimated SWP (kg m^{-2}) (second panel), the SSR detection mask (third panel), the estimated SSR (mm h^{-1}) (bottom panel).

to:

Figure 15: Greenland - 2016/04/24 - Maps of the HANDEL-ATMS module's output: the SWP detection mask (top panel), the estimated SWP (kg m^{-2}) (second panel), the SSR detection mask (third panel), the estimated SSR (mm h^{-1}) (bottom panel). The green dotted lines (bottom panel) represent the CloudSat track.